Showcasing research from Professor Andreas Lemmerer's laboratory, School of Chemistry, University of the Witwatersrand, Johannesburg, South Africa.

Polymorphism and photoluminescence seen in (2-amino-5-chloropyridine)·(9-anthracenecarboxylic acid)·(trinitrobenzene): a further example of the salt-cocrystal continuum observed by virtue of isolating multiple crystal forms

The image shows the three reactant powders, 1,3,5-trinitrobenzene (top left), 9-anthracenecarboxylic acid (top right), and 3-hydroxypyridine (bottom) that form a polymorphic ternary adduct that differs in the location of the acidic proton of the carboxylic acid. The bright orange needles of the molecular salt form and the deep red block-like crystal of the co-crystal form are an example of colour polymorphism that is caused by the neutral or charged nature of the components of the adduct. The two forms show vastly different photoluminescence behaviour.
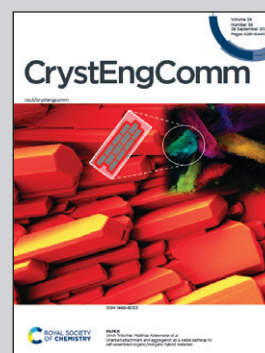
ROYAL SOCIETY
OF **CHEMISTRY**

rsc.li/crystengcomm

Check for updates

Polymorphism and photoluminescence seen in (2-amino-5-chloropyridine)·(9-anthracenecarboxylic acid)·(trinitrobenzene): a further example of the salt-cocrystal continuum observed by virtue of isolating multiple crystal forms†

Atiyyah Salajee, [iD] Caitlin Morrison, [iD] Rudolph Erasmus [iD] and Andreas Lemmerer [iD] *

Two polymorphic forms of the ternary adduct (2-amino-5-chloropyridine)·(9-anthracenecarboxylic acid)·(trinitrobenzene) were isolated. In both forms 9-anthracenecarboxylic acid displays a charge-transfer interaction with trinitrobenzene. Form **I** exhibits proton transfer from the carboxylic acid to the pyridine and forms a ternary molecular salt, while form **II** forms a ternary co-crystal. Form **I** crystallises out in acetonitrile, whilst form **II** crystalizes out in methanol. The two forms occur as concomitant pairs when crystallised from a variety of solvents. Form **I** crystallises as orange needles and form **II** crystallises as red blocks. Differential scanning calorimetry indicates that form **II** is the thermodynamically most stable form, and form **I** is the kinetically favoured form. Form **I**, being a molecular salt, luminesces whilst form **II**, being a cocrystal, does not luminesce. The two polymorphs are a further illustration of the salt/cocrystal continuum.

The design and synthesis of multi-component adducts has become an area of great interest in recent years due to their potential of enhancing the physiochemical properties of the starting components. Designing and isolating multi-component adducts is a delicate process since crystallisation is essentially a purification technique, which will often preferentially result in the formation of crystals of the individual starting materials.[1] Desiraju and co-workers[2] have been at the forefront of developing design strategies for the synthesis of higher order cocrystals, including ternary (three-component) cocrystals,[1,3,4]

Jan Boeyens Structural Chemistry Laboratory, Molecular Sciences Institute, School of Chemistry, University of the Witwatersrand, Private Bag 3, PO Wits, 2050, Johannesburg, South Africa. E-mail: Andreas.Lemmerer@wits.ac.za

quaternary (four-component) cocrystals,[5–7] and more recently quinary/quintinary (five-component)[6,7] and senary (six-component)[8] solid-solution cocrystals. In the past few years, many other research groups have also synthesized and studied ternary and quaternary cocrystals.[9–12] To hold the starting components of these higher order cocrystals together, intermolecular interactions are employed. In most instances hydrogen bonding is coupled with other types of intermolecular interactions such as halogen bonding,[4,9] charge transfer,[10,13,14] and stacking interactions.[1] In this paper ternary adducts were synthesized using the method developed in our research group, whereby a combination of hydrogen bonding and charge transfer interactions are used to combine the three starting components.[15] The electron poor trinitrobenzene (**tnb**) readily combines with the electron rich 9-anthracenecarboxylic acid (**9aca**) to form a charge transfer (CT) adduct. The third molecule is included through strong hydrogen bonding with the carboxylic acid of the **9aca**. Pyridines were found to be reliable hydrogen bond acceptors since the lone pair on the nitrogen atom readily bonds with the carboxylic acid proton. Ten different pyridine derivatives were utilised, which gave rise to either ternary co-crystals or ternary molecular salts.[15] Subsequently, it was found that by performing a polymorph screening study on one of these ternary molecular salts three polymorphs of the ternary molecular salt (2-aminopyridinium)·(9-anthracenecarboxylate)·(trinitrobenzene) were discovered.[16] Continuing in this vain and focusing on the pyridine derivative, 2-amino-5-chloro-pyridine (**2a5clp**), we set out to search for polymorphs for this ternary adduct. A polymorph is a solid crystalline phase of a given adduct which results from the possibility of at least two different arrangements of the molecules of that adduct in the solid state.[17] Both unimolecular and multi-component solids can exhibit polymorphism. Two polymorphs of the ternary adduct (2-amino-5-chloropyridine)·(9-anthracenecarboxylic acid)·(trinitrobenzene) were isolated

(Fig. 1). Form **I** exhibits proton transfer from the carboxylic acid of the **9aca** to the nitrogen atom of the pyridine ring to form a ternary molecular salt. In form **II** the proton remains on the carboxylic acid and a neutral ternary co-crystal is formed. Salt/cocrystal polymorphism has been encountered for binary adducts such as: isonicotinamide and citric acid,[18] sulfamethazine and saccharine,[19] and dinitrobenzoic acid and haloanilines,[20] but no cases have been found in the literature for ternary adducts, which makes this the first ternary adduct to exhibit salt/cocrystal polymorphism. Cocrystals and salts are both multicomponent crystals that differ based on the position of the proton between the acid and the base.[21] For salts complete proton transfer occurs from the acid to the base, whereas for a cocrystal proton transfer is absent with the proton being retained by the acid. To predict whether the outcome of a co-crystallisation experiment will be a cocrystal or a salt, a "pK_a rule" has been proposed which utilises the ΔpK_a [*i.e.*, pK_a (protonated base)–pK_a (acid)] of the adduct. A smaller ΔpK_a (less than 1) indicates a greater chance of obtaining a cocrystal, whilst a larger ΔpK_a (around 2 or 3) leads to a greater chance of obtaining a salt.[21,22] Accordingly, there exists a region of uncertainty around ΔpK_a = 1 where the extent of proton transfer is not predictable and the possibility of obtaining a cocrystal or a salt is very similar.[22] Acid–base adduct with similar pK_a values will fall into this region. For these adduct, both ΔpK_a values and the crystalline environment will determine the extent of proton transfer and hence cocrystal or salt formation.[21]

For slow evaporation at room temperature, with the use of a single solvent, form **I** (orange) would most commonly crystallise out, with only a few instances where both forms appeared concomitantly. When solvent mixtures were used at room temperature, forms **I** and **II** would occur mostly as concomitant pairs, with form **I** crystallising out first. For evaporation at a raised temperature (in the oven at 36 °C), form **II** (red) was the most common form to crystallise out, with a few instances where either only form **I** occurred or both forms occurred concomitantly. Note that differing solvent ratios may have also played a role in the polymorph that formed. A summary of the experimental procedure can be found in the supporting information. Both polymorphs were isolated at room temperature and their structures determined using single crystal X-ray diffraction. Crystallographic data, powder X-ray diffraction patterns and infrared spectra of the two polymorphs are given in the ESI.†
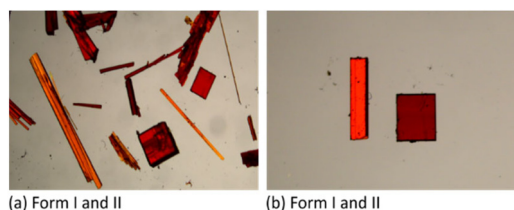

(a) Form I and II   (b) Form I and II

Fig. 1 Orange needles of form I and red blocks of form II.

Crystal structures of the two polymorphs were obtained from SCXRD and the assignments of the carboxylic proton required further experiments. The X-ray difference Fourier map of form **I** (Fig. S2†) shows electron density close to N4 of the pyridine, which suggests that a proton is attached to N4. The highest residual Q-peak is 0.95 Å away from the pyridinium nitrogen labelled N4. Further evidence of deprotonation of the carboxylic acid, now carboxylate, is seen in the C–O bond distances: C7–O8 is 1.2433(18) Å and C7–O7 is 1.2695(18) Å. This gives a ratio of 1.021, indicative of a carboxylate anion. However, when freely refining the position of the H atom from the difference Fourier map, a long N–H distance of over 1 Å was found. Closer inspection of the difference map contours shows that the electron density does extend slightly back towards the carboxylate group, indicating incomplete transfer. This is not unusual and has been reported for many binary adducts in the work of Childs *et al.*[21] To tentatively measure the percentage of the continuum, we applied a positional disorder model on form **I**, whereby we placed geometrically a H atom on the pyridinium N4 (H4A) and on the carboxylate O7 (H7). The relative site occupancy factors of the two H atoms refined to 0.69(3) in favour of the pyridinium position over the carboxylate position at 0.31(3). This resulted in a 0.03% improvement in the R-factor. Ultimately, we are going to simplify our discussion to treating form **I** as a molecular salt. Solution NMR carried out in acetone shows that proton transfer takes place. Unfortunately, we could only determine this in acetone since the main solvents we used in our crystallisation experiments contained exchangeable protons (see ESI† for detailed NMR assignment). Interestingly, the opposite behaviour is seen in form **II**. Here, the X-ray difference Fourier map of form **II** (Fig. S3†) shows electron density close to O7 of **9aca** and suggests that the proton is still attached to O7 of the carboxylic acid. In this case, the residual Q-peak is 0.95 Å away from the carboxylic acid. Similar to form **I**, the contour Fourier map shows slight electron density towards the pyridine N4. Again, we applied a positional disorder model and the site occupancies of two H atoms refined to a major component located on the carboxylic acid (0.69(3)) and a minor component on the pyridine (0.31(3)). Incidentally, the C–O bond lengths do show values indicative of a carboxylic acid, being 1.2131(14) Å for C7=O8 and 1.2997(13) Å for C7–O7, and for this reason we confine our discussion to treating form **II** as a co-crystal. There is a precedent for this continuum we are seeing in the two forms being on either end of the spectrum and is often seen in pairs of molecules where the ΔpK_a is close to 1. Considering our ternary adduct, the calculated pK_a of **9aca** is 3.49 and that of **2a5clp** is 4.67, which yields a calculated ΔpK_a value of 1.18. This pK_a difference of 1.18 falls within the narrow transition region between a cocrystal and a salt, and thus contributes to the cocrystal/salt continuum observed in this polymorphic pair. Form **I** crystallises in the space group $P\bar{1}$ whilst form **II** crystallises in the space group $P2_1/n$. The asymmetric units of the two polymorphs contain one
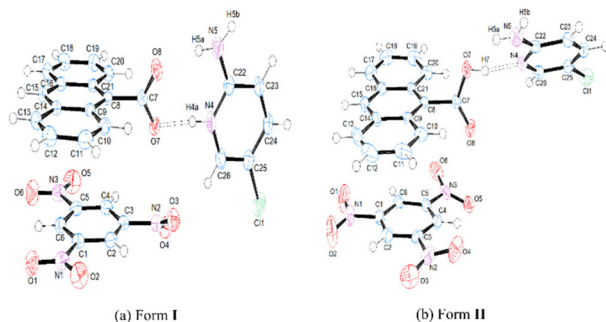
Fig. 2 Asymmetric unit of (a) form **I** the ternary salt and (b) form **II** the ternary cocrystal, indicating the numbering scheme, ellipsoids at 50% probability. Symmetry-independent hydrogen bonding interactions are shown as a dashed bond.

molecule each of the three starting components. In form **I**, the carboxylic acid group (O7–C7–O8) of **tnb** and the nitro group (O3–N2–O4) of **9aca**$^{(-)}$ are aligned on top of each other (Fig. 2a). In form **II**, the nitro group of **tnb** is shifted to the right, leaving the carboxylic acid of **9aca** to lie on top of a C–H bond (Fig. 2b). In both polymorphs, **tnb** acts as the acceptor in a $\pi \cdots \pi$ CT interaction with the aromatic system of **9aca**. Taking under consideration hydrogen bonding, in form **I** the **2a5clp**$^{(+)}$ cation is bonded to **9aca**$^{(-)}$ anion through a charge-assisted N$^{(+)}$–H$\cdots$O$^{(-)}$ hydrogen bond from the protonated pyridine to the carboxylate and through a second charge-assisted N–H$\cdots$O$^{(-)}$ hydrogen bond from one of the hydrogen atoms (H5A) of the amine to the same carboxylate to form an $R_2^2(8)$ ring (Fig. 3a). The second hydrogen atom H5B does not form a hydrogen bonded interaction. Form **II** has the **2a5clp** molecule hydrogen bonded to **9aca** via a neutral O–H$\cdots$N hydrogen bond from the carboxylic acid to the pyridine and via another neutral N–H$\cdots$O hydrogen bond from the hydrogen of the amine to the same oxygen of the carboxylic acid thus forming an $R_2^2(7)$ ring (Fig. 3b). The intermolecular potentials of the two polymorphs differ since there are two unique types of intermolecular interactions in these adducts. A UNI force field in the *MERCURY* package

can be used to make qualitative comparisons of the intermolecular potentials in the two polymorphs. The strongest interactions are the CT interactions. In form **I**, **tnb** has intermolecular potentials of −59.2 and −65.0 kJ mol^{-1} respectively with the neighbouring two **9aca**$^{(-)}$ anions on either side of **tnb** (Fig. S4†). The next strongest interaction in form **I** is found in the charge-assisted hydrogen bond of the **9aca**$^{(-)}$ anion to the **2a5clp**$^{(+)}$ cation, at −18.2 kJ mol^{-1}. In form **II**, **tnb** has intermolecular potentials of −59.1 and −64.1 kJ mol^{-1} respectively with its neighbouring **9aca** molecules (Fig. S5†). The third strongest interaction in form **II** is found in the bond between two **2a5clp** molecules, at −32.6 kJ mol^{-1}. The next strongest interaction in form **II** is found in the hydrogen bond between **9aca** and **2a5clp**, at −28.6 kJ mol^{-1}. There are $\pi \cdots \pi$ interactions between the pyridine molecules in form **II** (the co-crystal). The distance between the pyridine molecules is 3.36 Å. In form **I** (the salt) the distance between the pyridine molecules is around 6 Å, which is double that of the distance form **II**, and hence form **I** lacks the $\pi \cdots \pi$ interactions between its pyridine molecules.

The packing of the two polymorphs, as shown in Fig. 4, displays just how different they are. Form **I** has the **2a5clp**$^{(+)}$ cations forming a wave-like pattern, along the *b*-axis, in between rows of (**9aca**$^{(-)}$)·(**tnb**) CT dimers. Form **II** has the **2a5clp** molecules in single rows, along the *a*-axis, in between the rows of the (**9aca**)·(**tnb**) CT dimers.

The determination of the melting points and enthalpies of fusion of polymorphs are important factors since they will determine which form is the most thermodynamically stable. Differential scanning calorimetry (DSC) traces of the two polymorphs are given in (Fig. 5). The DSC trace (red) of form **II** shows a single melting endotherm at 157.5 °C with the largest enthalpy of fusion of −55.5 kJ mol^{-1} (Table 1). Variable temperature single crystal X-ray diffraction (SCXRD) experiments of form **II** showed that the unit cell lengths and the cell volume remained constant as the temperature increased (Fig. S15 and S16†), which indicates that form **II**
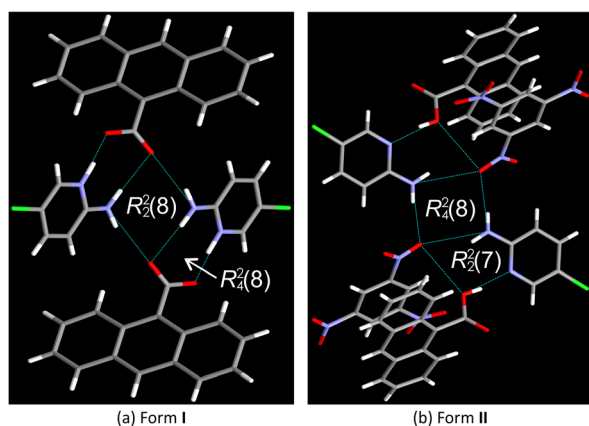

Fig. 3 The hydrogen bonded interactions in both forms, showing the graph set notation for each one.
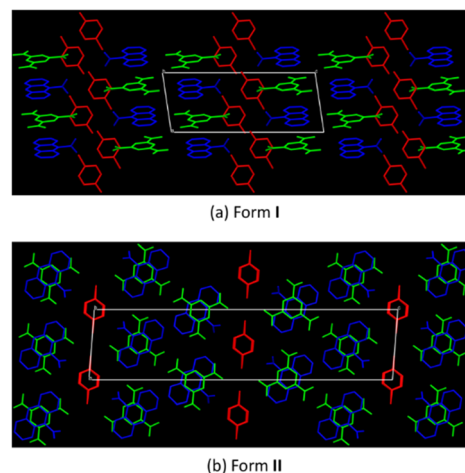

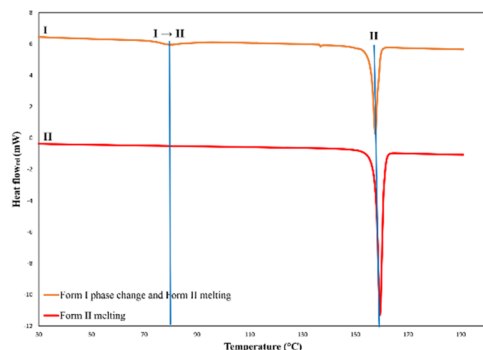**Fig. 4** The packing of the two forms both shown down the *b*-axis.

Fig. 5 Representative DSC traces of samples of forms I and II. Exotherms are up.

Table 1 Results of DSC experiments[a]

Polymorph	T_{onset}/°C	T_{peak}/°C	Enthalpy/kJ mol^{-1}
Form I → II	73.5 ± 1.1	79.4 ± 0.9	−7.7 ± 0.1
Form II	157.5 ± 0.1	159.4 ± 0.2	−55.5 ± 1.0

[a] All values were calculated from triplicate measurements.

does not undergo any phase changes and that the melting point measured on the DSC is indeed that of form II. The DSC trace (orange) of form I shows a phase transition at 73.5 °C, with an enthalpy of −7.7 kJ mol^{-1}, and thereafter a melting endotherm at 156.1 °C, which is consistent with the melting of form II. Variable temperature SCXRD data for form I could only be collected until the phase change (Fig. S13 and S14†) since the crystal had cracked when undergoing the phase change and was no longer X-ray diffraction quality. Furthermore, a sample of form I was heated on the DSC until 100 °C then cooled back to 25 °C to determine whether the phase change from form I to form II was reversible or irreversible. The DSC trace of this sample (Fig. S11†) shows a single endotherm upon heating, which corresponds to the phase change to form II, and no further endotherms or exotherms upon cooling. This indicates that form I undergoes an irreversible phase transition to form II. This is consistent with the results obtained from hot stage microscopy where a phase change was observed for form I wherein the crystal changed colour from orange to red. Infrared spectroscopy (IR) and powder X-ray diffraction (PXRD) were also used to verify this phase change. A sample of form I was heated on the DSC and allowed to undergo the phase transition. IR spectra and PXRD patterns of this sample were then measured and compared to those of pure form I and form II. Both the IR spectrum and PXRD pattern of this sample resemble those of form II (Fig. 6 and S10†), which proves that indeed form I transforms to form II. Additional DSC scans were done for form I, at increased scan rates (≥100 K min^{-1}), in an attempt to overcome the kinetics of the phase transition and determine the melting point of form I. However, the phase change of form I to form II was persistent and hence the melting point of form I could not be determined. The DSC trace of form I (Fig. 5) shows an endothermic transition prior to the melting endotherm, which suggests that form II is the thermodynamically stable form. Slurry experiments were conducted to verify this observation. Red and orange crystals of forms I and II respectively, were placed in a vial with hexane. The vial was sealed, and the mixture left to stir for 24 h. Thereafter, the vial was opened to allow the remaining hexane to evaporate (further experimental details are given in the ESI†). A red

powder formed. DSC scans were done on these powders and their DSC traces (Fig. S12†) show a single melting endotherm around 157 °C, which is consistent with that of form II, hence form II is the most thermodynamically stable form. Finally, according to the heat of transition rule of Burger and Ramberger,[23] the presence of an endothermic transition in the DSC trace of form I (Fig. 5) indicates that the polymorphs are related enantiotropically.

The colour polymorphism exhibited by the orange form I and the red form II was investigated using photoluminescence (PL) spectroscopy and diffuse reflectance spectroscopy (DRS). The PL spectra of form I (Fig. S17†) shows a clear broad red emission spectrum between 525 nm and 900 nm, with the primary peak centred on 650 nm. The PL spectra of form II (Fig. S17†) shows very little to no luminescence under the exact same measurement conditions. The colour polymorphism is thus strongly associated with PL emission for the orange form I sample while the red form II sample shows no PL. It is likely that the presence of a cation and anion pair in the molecular salt (form I), where 'incomplete' proton transfer from the carboxylic acid to the pyridine takes place, is associated with the origin of the PL in this sample, but this hypothesis is a subject for future investigations. The diffuse reflectance spectra of forms I and II reflect the visual colour difference of the two samples. Form I (orange) has a DRS curve with inflection point at 565 nm, while for form II (red) this point is at 596 nm (Fig. 7). Form II thus absorbs light further into the red part of the visible spectrum, corresponding with its distinct red visual appearance, while form I does not absorb all orange light, in keeping with its distinct orange visual appearance.
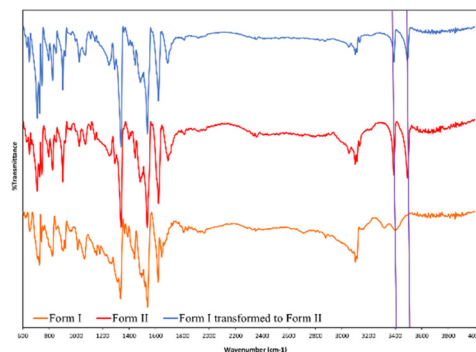

Fig. 6 Comparison of the infrared spectra of forms I and II, and the spectrum of a sample of form I, heated and transformed to form II on the DSC (see description in main article). The two peaks indicated by the solid purple lines are convenient for showing alikeness and difference (see ESI† for a full spectral analysis).
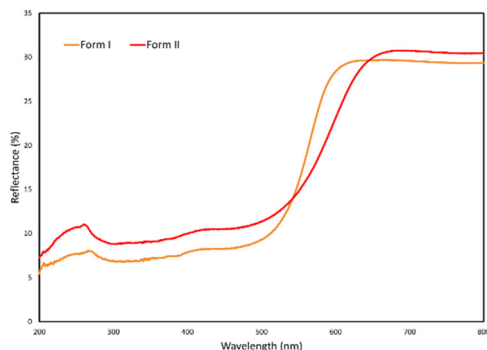
Fig. 7 Diffuse reflectance spectra of forms I and II.

The design of ternary adducts is a delicate process as combining three molecules into a single crystalline lattice requires thoughtful consideration when choosing the three molecules, bearing in mind the different types of intermolecular interactions that are at play. Hydrogen bonding is the most common interaction used and is often combined with other intermolecular interactions, such as charge transfer and halogen bonding. In this work, charge transfer interactions were used to combine the electron poor **tnb** with the electron rich aromatic system of **9aca**. The use of a base with a similar pK_a as the acid allowed for the formation of a salt or a cocrystal. Two polymorphs of the ternary adduct (2-amino-5-chloropyridine)·(9-anthracenecarboxylic acid)·(trinitrobenzene) were isolated, with form **I** a salt and form **II** a cocrystal. The polymorphs exhibit an enantiotropic relationship with form **I** undergoing a phase change to the thermodynamically most stable form **II**. This phase change of the ternary molecular salt (form **I**) to the ternary cocrystal (form **II**) is interesting since it highlights the notion that the extent of proton transfer in the solid state for acid–base adducts with similar pK_a values is unpredictable, although subject to influence by the molecular environment,[21] and thus showcases the salt/cocrystal continuum. The pathway has been paved for successfully synthesizing ternary adducts and exploring the existence of polymorphism in these adducts. In future, similar principles can be applied to synthesize and characterize quaternary adducts.

Conflicts of interest

There are no conflicts to declare.

Acknowledgements

Notes and references

1 S. Chakraborty, L. Rajput and G. R. Desiraju, *Cryst. Growth Des.*, 2014, **14**, 2571–2577.
2 N. A. Mir, R. Dubey and G. R. Desiraju, *Acc. Chem. Res.*, 2019, **52**, 2210–2220.
3 H. Jain, D. Sutradhar, S. Roy and G. R. Desiraju, *Angew. Chem.*, 2021, **133**, 12951–12956.
4 S. Tothadi and G. R. Desiraju, *Chem. Commun.*, 2013, **49**, 7791–7793.
5 R. Dubey, N. A. Mir and G. R. Desiraju, *IUCrJ*, 2016, **3**, 102–107.
6 N. A. Mir, R. Dubey and G. R. Desiraju, *IUCrJ*, 2016, **3**, 96–101.
7 M. Rajkumar and G. R. Desiraju, *IUCrJ*, 2021, **8**, 178–185.
8 M. Paul, S. Chakraborty and G. R. Desiraju, *J. Am. Chem. Soc.*, 2018, **140**, 2309–2315.
9 F. Topić and K. Rissanen, *J. Am. Chem. Soc.*, 2016, **138**, 6610–6616.
10 C. C. Seaton, N. Blagden, T. Munshi and I. J. Scowen, *Chemistry*, 2013, **19**, 10663–10671.
11 L. Hou, L. Gao, W. Zhang, X.-J. Yang and B. Wu, *Cryst. Growth Des.*, 2021, **21**, 2837–2843.
12 M. Rajkumar, *Cryst. Growth Des.*, 2021, **21**, 3547–3553.
13 T. Hill, D. C. Levendis and A. Lemmerer, *Acta Crystallogr., Sect. E: Crystallogr. Commun.*, 2018, **74**, 113–118.
14 T. N. Hill, D. C. Levendis and A. Lemmerer, *J. Mol. Struct.*, 2018, **1168**, 28–38.
15 T. Hill, R. M. Erasmus, D. C. Levendis and A. Lemmerer, *CrystEngComm*, 2019, **21**, 5206–5210.
16 A. Lemmerer, *CrystEngComm*, 2020, **22**, 6091–6095.
17 J. Bernstein, *Polymorphism in Molecular Crystals 2e*, International Union of Crystal, 2020.
18 P. Stainton, T. Grecu, J. McCabe, T. Munshi, E. Nauha, I. J. Scowen and N. Blagden, *Cryst. Growth Des.*, 2018, **18**, 4150–4159.
19 S. R. Perumalla, C. Wang, Y. Guo, L. Shi and C. C. Sun, *CrystEngComm*, 2019, **21**, 2089–2096.
20 C. L. Jones, J. M. Skelton, S. Parker, P. R. Raithby, A. Walsh, C. C. Wilson and L. H. Thomas, *CrystEngComm*, 2019, **21**, 1626–1634.
21 S. L. Childs, G. P. Stahly and A. Park, *Mol. Pharmaceutics*, 2007, **4**, 323–338.
22 A. Aramini, G. Bianchini, S. Lillini, S. Bordignon, M. Tomassetti, R. Novelli, S. Mattioli, L. Lvova, R. Paolesse, M. R. Chierotti and M. Allegretti, *Pharmaceuticals*, 2021, **14**, 555.
23 A. Burger and R. Ramberger, *Microchim. Acta*, 1979, **72**, 259–271.